catalysts

MDPI

Article

Effect of Ce/Y Addition on Low-Temperature SCR Activity and SO_2 and H_2O Resistance of MnO_x/ZrO_2/MWCNTs Catalysts

Lifu Dong [1], Yinming Fan [1], Wei Ling [1], Chao Yang [1] and Bichun Huang [1,2,3,*]

1. School of Environment and Energy, South China University of Technology, Guangzhou Higher Education Mega Centre, Guangzhou 510006, China; donglifu06@163.com (L.D.); YMing_Fan2015@163.com (Y.F.); violin0544@163.com (W.L.); yc0835@163.com (C.Y.)
2. Guangdong Provincial Key Laboratory of Atmospheric Environment and Pollution Control, South China University of Technology, Guangzhou Higher Education Mega Centre, Guangzhou 510006, China
3. The Key Lab of Pollution Control and Ecosystem Restoration in Industry Clusters, Ministry of Education, South China University of Technology, Guangzhou Higher Education Mega Centre, Guangzhou 510006, China

* Correspondence: cebhuang@scut.edu.cn; Tel.: +86-20-3938-0516

Academic Editors: Tian-Yi Ma, Jian-Rong (Jeff) Li and Cláudia Gomes Silva
Received: 10 March 2017; Accepted: 23 May 2017; Published: 8 June 2017

Abstract: The effects of SO_2 and H_2O on the low-temperature selective catalytic reduction (SCR) activity over MnO_x/ZrO_2/MWCNTs and MnO_x/ZrO_2/MWCNTs catalysts modified by Ce or Y was studied. MnCeZr and MnYZr catalysts reached nearly 100% and 93.9% NO_x conversions at 200 °C and 240 °C, respectively. They displayed a better SO_2 tolerance, and the effect of H_2O was negligible. The structural properties of the catalysts were characterized by XRD, H_2-TPR, XPS, and FTIR before and after the reaction. The results showed that Ce could increase the mobility of the oxygen and improve the valence and the oxidizability of manganese, while the effect of Y was the opposite. This might be the main reason why the catalytic activity of MnCeZr was better than MnYZr in the presence or absence of SO_2 and H_2O. Doping Ce or Y broadened the active temperature window. Ce or Y, which existed in the catalysts with a high dispersion or at the amorphous state, preferred to react with SO_2 to form sulfate species, and protected the manganese active sites from combing with SO_2 to some extent, which coincided with the theory of ionic polarization.

Keywords: ionic polarization; low-temperature SCR; MnO_x/ZrO_2/MWCNTs; SO_2; poisoning resistance

1. Introduction

Selective catalytic reduction (SCR) technology is widely used to remove nitrogen oxides from flue gas and has the advantages of stability and efficiency [1,2]. Catalysts are a crucial factor in SCR technology and directly determine the efficiency of the system. However, conventional commercial catalysts (V_2O_5-WO_3(MoO_3)/TiO_2) have a relatively narrow temperature window of 300–400 °C, and they are not active at the typical temperature of flue gases (≤250 °C) in the catalytic bed located downstream of the desulfurizer and particulate removal device, and will be deactivated by SO_2 and H_2O [1,3,4]. Therefore, there is great interests in developing new catalysts which are active at relatively low temperatures and have better resistance to SO_2 and H_2O. Some transition metal oxides (Fe, V, Cr, Cu, Mn) supported on catalysts have been found with high activities at low temperatures [5–9]. Among them, Mn-based catalysts have been investigated in depth via several means because manganese oxides contain various kinds of labile oxygen, which is beneficial for the fulfillment of the catalytic cycle [9–16]. MnO_2 is the most active species among MnO_2, Mn_5O_8, Mn_2O_3, and Mn_3O_4 [17].

Carbon nanotubes (CNTs) have been extensively studied in low temperature SCR reactions based on their unusual physical and chemical proprieties, such as their unique electronic properties, special structure, higher surface areas, and so on [18,19]. In our previous study, Zr and Mn supported on multi-wall carbon nanotubes (MWCNTs) for NH_3-SCR reactions showed high activity at low temperatures. The modification of zirconium could increase the dispersion of MnO_x on the MWCNTs, the specific surface area, the total pore volume and the average pore size of the catalysts. The modification of zirconium could also enhance the atomic concentration of chemisorbed oxygen on the catalyst surface and promote the conversion of Mn^{3+} to Mn^{4+}. Therefore, the amounts of the active sites on the surface and the redox ability of the catalysts were improved. Additionally, the amounts and strength of acid on the surface of the catalysts were increased. However, their SCR activity was reduced in the presence of SO_2 and H_2O. Catalysts were deactivated by the formation of $(NH_4)_2SO_3$ and NH_4HSO_4 which did not decompose at low temperatures and blocked the pore channels of the catalysts or the competitive adsorption with NO [20–26]. H_2O inhibited the SCR reaction due to its competitive adsorption with NH_3 on the Lewis sites [27,28].

According to the theory of ionic polarization [29], the formation of a metal sulfate can be regarded as the inverse process of metal sulfate decomposition (Equation (1)). If $MeSO_4$ is harder to decompose, $MeSO_4$ is more stable and it is easier for Me and SO_3 to form $MeSO_4$. If the decomposition temperature of $MeSO_4$ is higher than that of manganese sulfate, Me prefers to combine with SO_3 over Mn. The decomposition temperature of ceric sulfate (973 °C) and yttrium sulfate (976 °C) were higher than manganese sulfate (814–928 °C), which indicates that ceric sulfate and yttrium sulfate are more easily formed than manganese sulfate, and manganese sites over these catalysts can be protected. Therefore, Ce and Y were selected to improve the tolerance of catalysts caused by SO_2 and H_2O.

$$MeSO_4 \rightarrow MeO(s) + SO_3 \tag{1}$$

MnO_x-CeO_x/ZrO_2/MWCNTs(MnCeZr) and MnO_x-YO_x/ZrO_2/MWCNTs(MnYZr) catalysts were prepared in this study by using the step impregnation method. The role of Ce/Y, the influences of SO_2 and H_2O over these MnO_x/ZrO_2/MWCNTs(MnZr), MnCeZr, and MnYZr, and finally the structural property and reducibility of the catalysts are discussed. X-ray powder diffraction (XRD), H_2 temperature programmed reduction (H_2-TPR), X-ray photoelectron spectroscopy (XPS), and Fourier transform infrared (FTIR) spectroscopy were used in this study.

2. Results and Discussion

2.1. SCR Performance

NH_3-SCR activity experiments over the MnZr, MnCeZr, and MnYZr catalysts were carried out, as depicted in Figure 1. The results showed that the activities of the catalysts were significantly improved and had obvious differences in NO_x conversion with the increasing temperature. Nearly 100% of NO_x conversion over the MnCeZr catalyst occurred at 200 °C, while the maximum NO_x conversions over MnZr and MnYZr were 93.6% at 200 °C and 99.3% at 240 °C, respectively. The NO_x conversions remained above 90% over MnZr, MnCeZr, and MnYZr catalysts in the temperature range of 190–220 °C, 170–270 °C, and 220–270 °C, respectively. According to the experimental data, the addition of Ce on MnZr catalysts improved the catalytic activity significantly while Y gave the opposite effect. However, they both enlarged the active temperature windows of the catalysts.

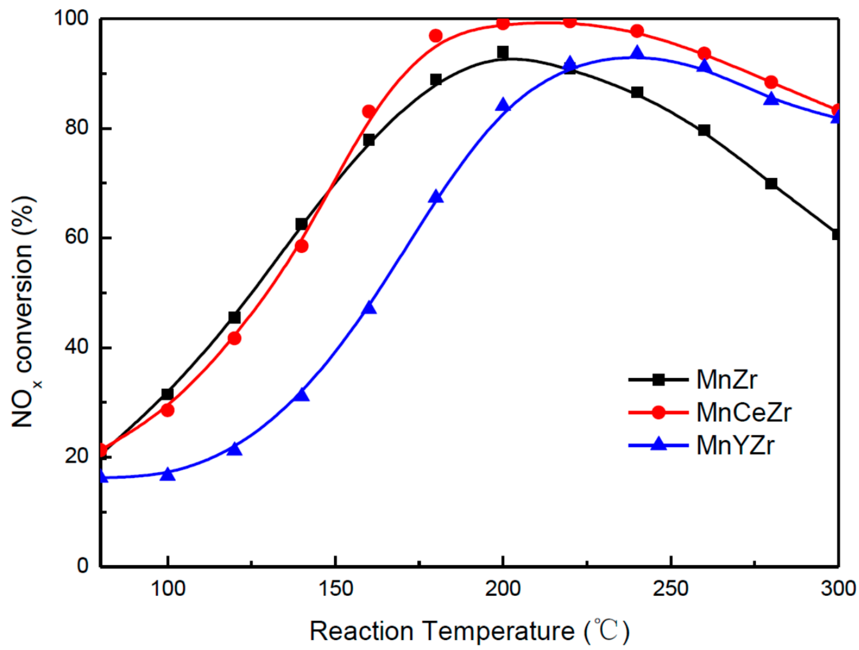

Figure 1. NO_x conversion of Ce-, Y-doped MnO_x/ZrO_2/MWCNTs catalysts as a function of temperature reaction condition: 0.06% NO; 0.06% NH_3; 3% O_2; Ar balance, gas hour space velocity (*GHSV*) = 40,000 h^{-1}.

2.2. Effect of SO_2 on SCR Catalytic Activity

Figure 2 shows the effect of SO_2 on the NO_x conversion over MnZr, MnCeZr and MnYZr catalysts. The NO_x conversion decreased as SO_2 was introduced into the system. The NO_x conversion of MnZr showed a relatively faster deactivation, and decreased from 88.6% to 37.4% after 20 min in the presence of SO_2. In contrast, the NO_x conversions of MnCeZr and MnYZr decreased to 85% and 74.8%, respectively. Their NO_x conversion declined slowly and were maintained above 60% for the next 105 min, respectively. It can be deduced from Figure 2 that the poisoning of SO_2 on the SCR activity of the catalysts was most likely caused by the sulfation of the active sites. This coincides with the work of Pan [24]. The addition of Ce or Y on MnZr slowed the sulfation progress and resulted in the improvement of SO_2 resistance. Furthermore, it was evident that the catalytic activity of MnCeZr was better than that of MnYZr in the reactions. When SO_2 was absent from the feed gas, the NO_x conversion could not be recovered. This indicated that the deactivation caused by SO_2 was irreversible.

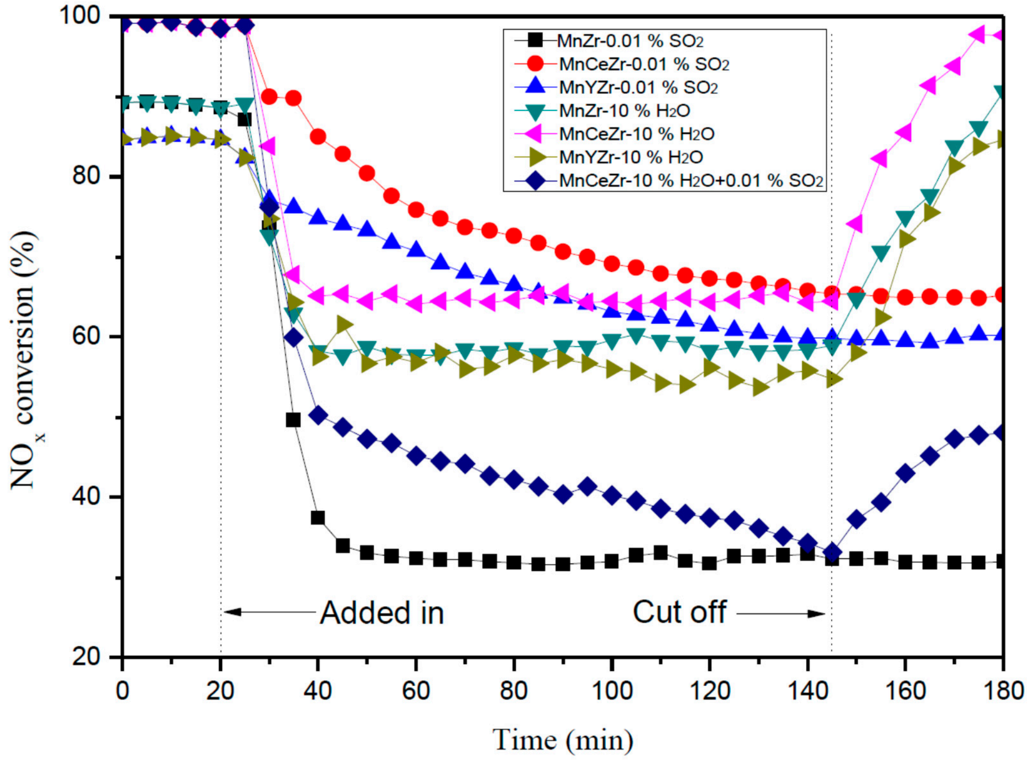

Figure 2. Effect with/without SO_2 or H_2O on the SCR activity of catalyst reaction conditions: 0.1% NO; 0.1% NH_3; 5% O_2; 10% H_2O (when added); 0.01% SO_2 (when added); and 200 °C, Ar balance.

2.3. Effect of H_2O on SCR Catalytic Activity

Figure 2 shows that when 10 vol. % of H_2O was continuously introduced into the system, the NO_x conversions on MnZr, MnCeZr, and MnYZr had a significant drop in a short time and then remained stable at this level. The NO_x conversions on MnCeZr and MnYZr decreased to about 70% and 60%, respectively. When H_2O was completely removed from the feed gas, the activity could almost completely recover to its original level. H_2O caused a decline in activity and the inhibiting effect of H_2O on the SCR activity of the catalysts was reversible.

2.4. Effect of H_2O and SO_2 on SCR Catalytic Activity

Figure 2 further shows that when 0.01 vol. % of SO_2 and 10 vol. % of H_2O were introduced into the system, a sharp decline of the NO_x conversion from 98.91% to 50.24% on MnCeZr was observed, and then the NO_x conversion dropped slowly in the rest time. According to the experimental data, the coexistence of SO_2 and H_2O deactivated the catalysts more seriously than either in the presence of SO_2 or H_2O alone. Moreover, the activity was not recovered after cutting off H_2O + SO_2, implying that the coexistence of H_2O and SO_2 had a synergistic poisoning effect on the SCR activity.

2.5. XRD Results

Figure 3 displays the XRD patterns of different catalysts at wide diffraction angles. The XRD profiles of MnCeZr and MnYZr remained almost unchanged. ZrO_2 and MnO_x were the major species after the introduction of Ce or Y, respectively, which indicated that the loading of Ce or Y did not change the structure of MnZr. The only exception was that the XRD pattern of MnCeZr showed a weak peak at 47.5°, representing CeO_2 (PDF#34-0394). No other characteristic peaks of Ce and Y compounds over MnCeZr and MnYZr were observed, indicating that Ce and Y were well incorporated and dispersed in the catalysts, or that the formed compounds were not large enough to be detected.

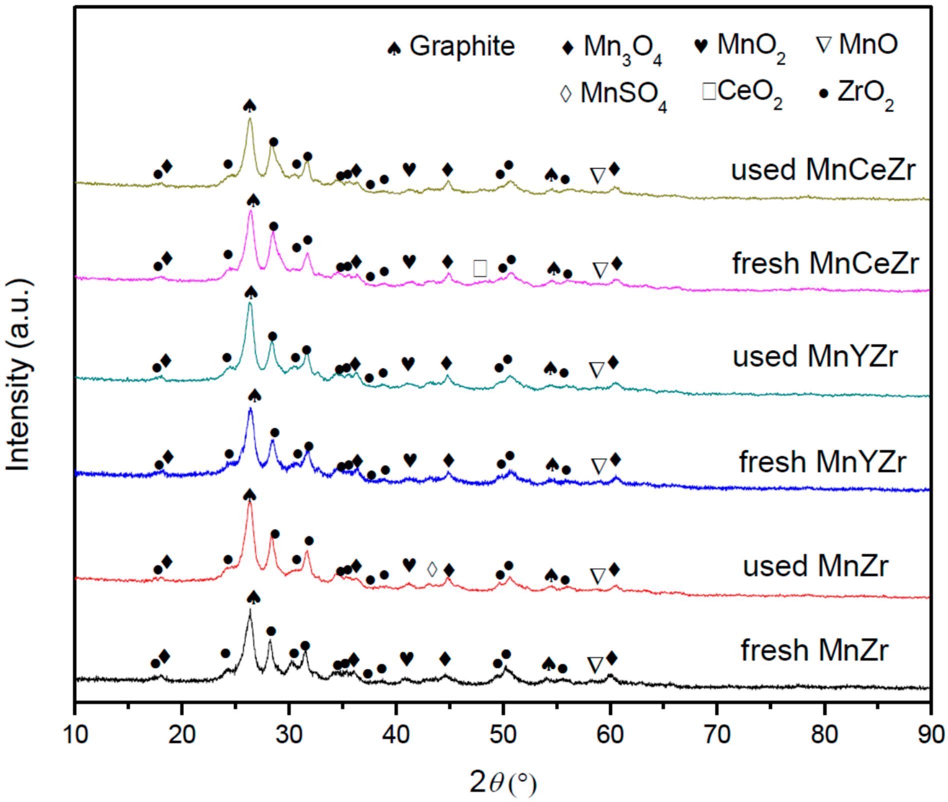

Figure 3. XRD patterns of catalysts before and after the reaction in the presence of SO_2.

Figure 3 displays the XRD patterns of the fresh and used catalysts with/without loading Ce or Y on MnZr. The peak that appeared at 42.7° can be assigned to the phases of $MnSO_4$ (PDF#35-0751) formed. With the SCR activity results (Figure 2), the newly formed crystal phases $MnSO_4$ on MnZr decreased the SCR activity. However, there were no detectable peaks of $MnSO_4$ for the used MnCeZr and MnYZr, indicating that these sulfate species may exist as amorphous species or do not reach the detection limit.

2.6. H_2-TPR Results

Figure 4 shows the H_2-TPR results of various fresh catalysts. The three catalysts all present three redox peaks in the temperature ranges of 100–200 °C, 250–400 °C, and 450–700 °C, which correspond to the reduction of the surface oxygen, MnO_2 to Mn_3O_4 and Mn_3O_4 to MnO, respectively [9,30]. The peak at 325 °C which corresponded to the reduction of MnO_2 to Mn_3O_4 played an important role in the reaction over MnZr [17,31]. It shifted to a lower temperature at 299 °C and a higher temperature at 344 °C over MnCeZr and MnYZr, respectively. Considering the SCR activity (Figure 1), this may have been due to the addition of Ce to MnZr, which improved the mobility of the oxygen as well as the valence and oxidization properties of manganese, while the addition of Y gave the opposite effect [32,33].

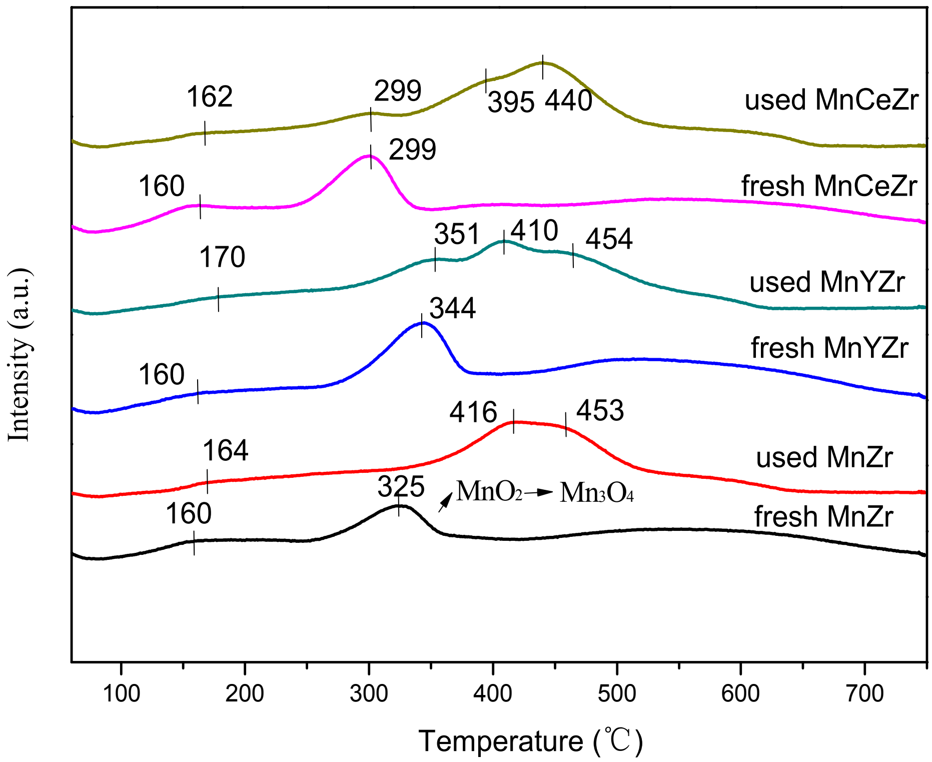

Figure 4. H_2-TPR profiles of catalysts before and after the reaction in the presence of SO_2.

Figure 4 displays the H_2-TPR results of the fresh and used catalysts when SO_2 was introduced to the system. In the case of the MnZr catalysts, the peak of MnO_2 to Mn_3O_4 at 325 °C disappeared while two new peaks at 416 °C and 453 °C appeared after the reaction under SO_2 flow. Based on the activity test and characterization results, the poisoning effect of SO_2 on the catalysts was directly related to the newly formed sulfate species, which decreased the mobility of the oxygen that led to a decrease in SCR activities [34]. With the addition of Ce or Y to MnZr, the reduction peak of MnO_2 to Mn_3O_4 did not disappear, but became weaker after the reaction under SO_2 flow. It may be deduced that the addition of Ce or Y inhibited the formation of sulfate species and protected the active sites to some extent.

2.7. XPS Results

The surface atomic compositions by XPS analysis are given in Table 1. It was noted that surface oxygen on the fresh MnZr catalysts was 7.96% and increased to 9.22% with the addition of Ce while the surface oxygen decreased to 7.23% with Y addition. This is in accordance with H_2-TPR results, which indicated that Ce improves the oxygen storage capacity of the catalysts while the effect of Y was opposite. Compared to the fresh catalysts, the manganese concentration in the catalysts declined by 31.3% (MnZr), 18.2% (MnCeZr), and 5.3% (MnYZr) after the reaction under SO_2 flow, respectively. The formation of sulfate species on the active sites reduced the amount of surface manganese, which was in accordance with the results of Luo's study [34]. The results also confirmed that the sulfation of the active sites was inhibited to some extent after loading Ce or Y. Naturally, some sulfur and nitrogen atoms were detected under the XPS measurement on the surface of the used catalysts, which confirmed that sulfate species were formed on the surface of the catalysts.

Table 1. Surface atomic concentration of catalysts before and after the reaction in the presence of SO_2.

Catalyst	Surface Atomic Concentration (%)							
	C	O	Mn	Zr	Ce	Y	S	N
Fresh MnZr	88.25	8.14	1.6	2.01	-	-	-	-
Fresh MnCeZr	86.98	9.22	1.32	1.72	0.76	-	-	-
Fresh MnYZr	89.91	7.23	0.75	1.89	-	0.22	-	-
Used MnZr	88.82	7.54	1.38	1.61	-	-	0.14	0.51
Used MnCeZr	88.66	7.78	1.09	1.56	0.52	-	0.15	-
Used MnYZr	88.53	7.71	0.71	1.66	-	0.18	0.14	1.07

The XPS spectra for the O 1s species is shown in Figure 5. The peaks at 529.8 and 531.8 eV correspond to the lattice oxygen (O_β) and the surface oxygen (O_α), respectively [35]. From the calculations, the ratio of $(O_\alpha)/(O_\alpha + O_\beta)$ in MnZr (46.1%) was lower than that in MnCeZr (52.4%) and MnYZr (72.6%), respectively. This is owing to the fact that loading Ce or Y increased the defects of metal oxides and oxygen vacancies. [36]. Figure 6 shows the XPS spectra for Mn 2p of the fresh and used catalysts after reacting with SO_2. Compared to the fresh catalysts, the Mn $2p_{1/2}$ and $2p_{3/2}$ peaks of the used MnZr catalysts (Figure 6a) moved from 653.4 eV and 642.2 eV to 654.1 eV and 642.7 eV, respectively. This was due to the sulfation of the manganese, which made the Mn $2p_{3/2}$ peak of the Mn/TiO_2 catalysts shift towards a higher binding energy (approximately 0.7 eV after SCR with SO_2), in accordance with the study of Jin [37]. When loading Ce or Y, the peaks were not significantly varied. The results also further confirmed that the sulfation of manganese was inhibited to some extent after loading Ce or Y. The Ce 3d XPS pattern (Figure S1) indicated that Ce existed as Ce^{4+} and Ce^{3+}. The characteristic peaks u, u'', u''', v, v'', and v''' corresponded to Ce^{4+}, and peaks u' and v' were attributed to Ce^{3+} [31]. From the calculations, the ratio of Ce^{4+}/Ce^{3+} in the used MnCeZr catalysts was lower (from 6.87% to 3.28% after SCR with SO_2), which indicated that Ce^{4+} was partially reduced to Ce^{3+}. The Y 3d XPS pattern (Figure S2) of MnYZr remained almost unchanged after reacting with SO_2, which may be interpreted as an indication that the valence of Y was not varied.

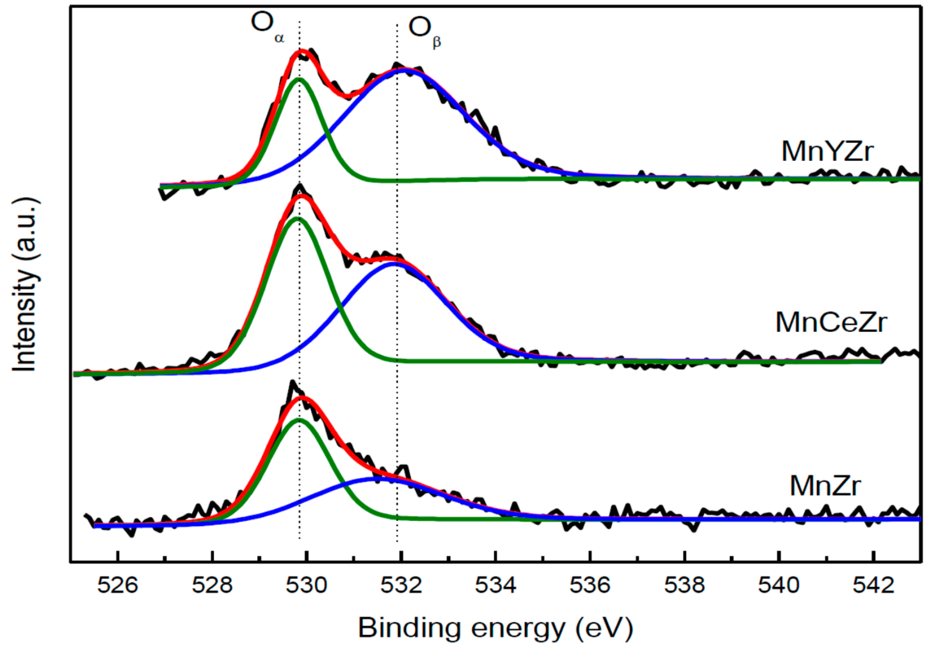

Figure 5. O 1s XPS spectra of catalysts before and after doping of Ce and Y.

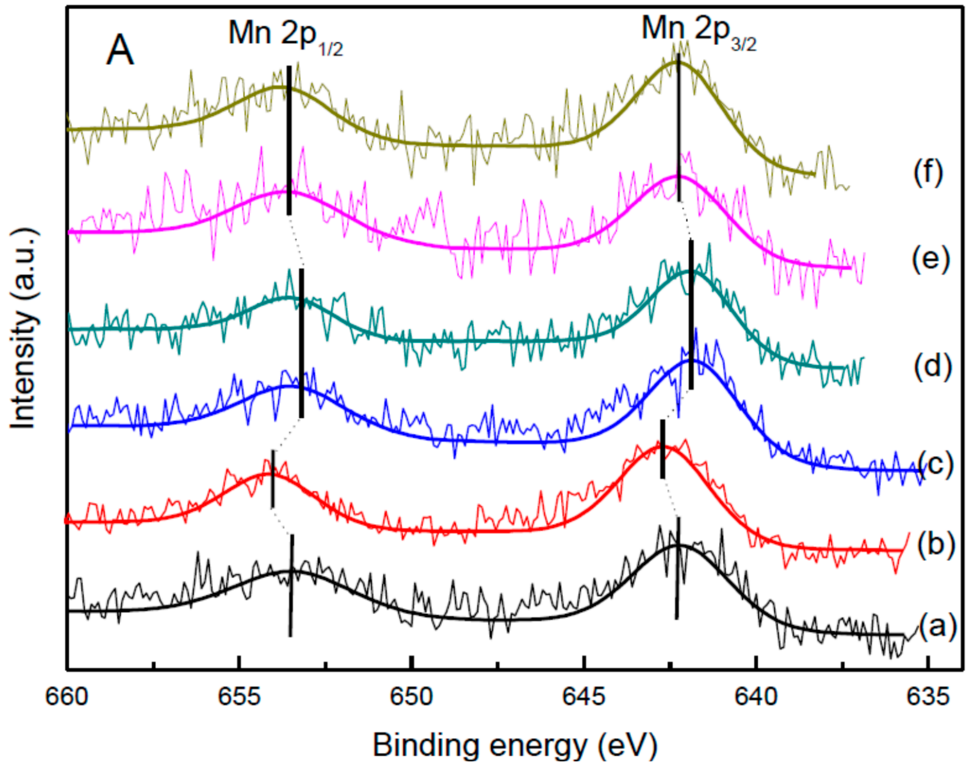

Figure 6. Mn 2p X spectra of catalysts before and after the reaction in the presence of SO_2. (**a**) Fresh MnZr; (**b**) used MnZr; (**c**) fresh MnCeZr; (**d**) used MnCeZr; (**e**) fresh MnYZr; (**f**) used MnYZr.

The sulfation of the active sites on the catalysts was the process of SO_2 combining with the surface oxygen, which was accompanied by changes in the surface oxygen. According to the results of Dupin's study [38], the binding energy of 527.7–530.6 eV corresponded to the lattice oxygen; 530.6–531.1 eV was ascribed to OH^-; and 531.1–532 eV was denoted as O^- which could supply the defects of lattice oxygen, such as the oxygen in Mn–O–Ce, Ce=O, and Mn–O–Y species. More than 532 eV was attributed to the weakly adsorbed oxygen in the surface. Surface oxygen of the fresh and used catalysts by XPS analysis is shown in Figure 7. According to the results of XPS, it was observed that the binding energy of 529.8 eV corresponding to the lattice oxygen exhibited the largest peak areas for all samples. Combined with the results of XRD indicating that there were many crystalline phases of ZrO_2, it was implied that the peak was attributed to the lattice oxygen of ZrO_2. The peaks at 531.2 eV and 532.5 eV of the MnZr catalysts were ascribed to O^- and the surface weakly adsorbed oxygen, respectively. Due to the sulfate ions formed after reacting with SO_2, these two peaks moved to 531.6 eV and 532.8 eV, respectively, while a new peak appeared at 530.6 eV, corresponding to OH^- at the same time. This was caused by the decomposition of the formed sulfate ions. This phenomenon was also observed on the catalysts after loading Ce or Y. The peak at 529.2 eV, which was ascribed to the disappearance of the oxygen of CeO_2 over the MnCeZr catalysts, indicated that a large number of CeO_2 was consumed after SCR with SO_2. Table 2 shows the proportions of different O species obtained by the peak fitting of the O 1s curves. The O 1s peaks were numbered as O 1s 1, O 1s 2, O 1s 3, and O 1s 4, from low to high binding energy. According to the experimental data, the lattice oxygen and the surface oxygen showed a significant decrease after reacting with SO_2, while OH^- and O^- increased. This may be caused by the hydrolyzation of the sulfate ions.

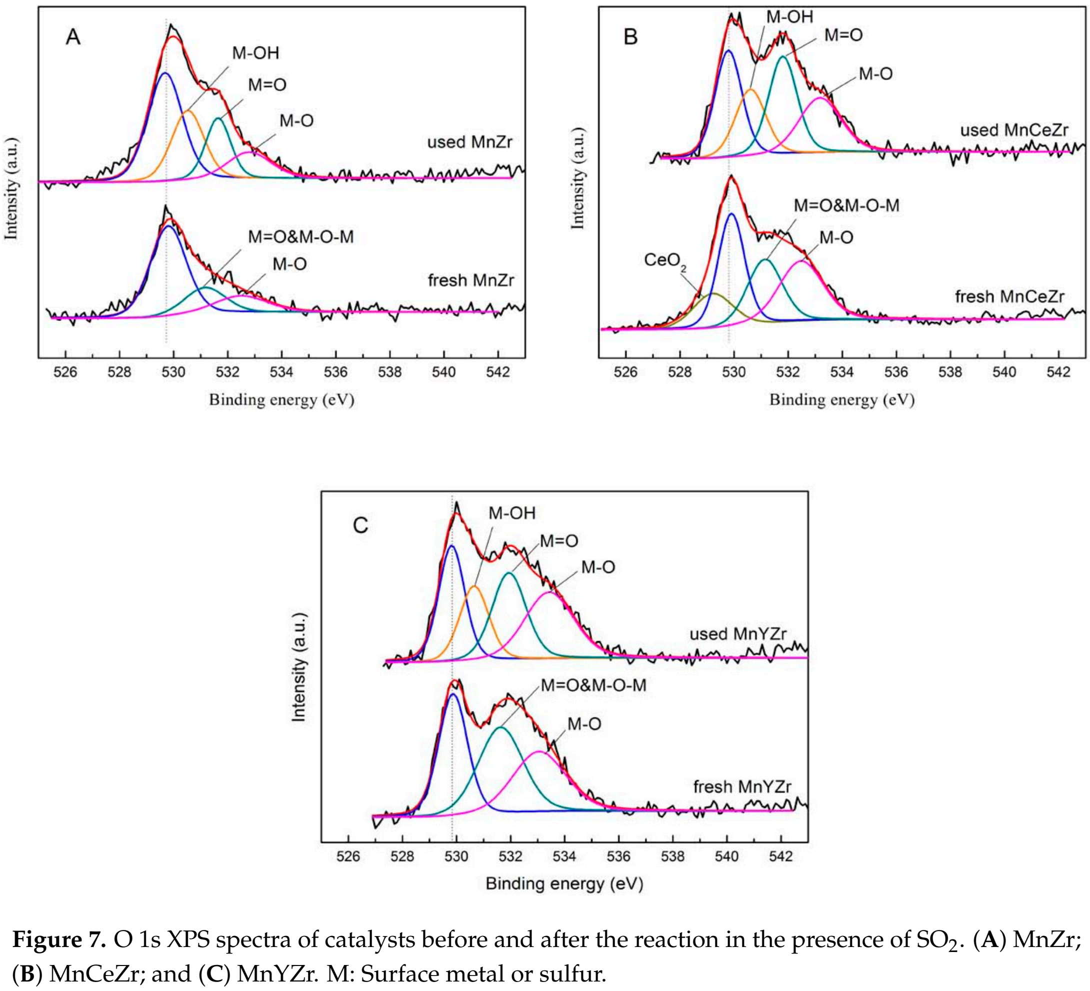

Figure 7. O 1s XPS spectra of catalysts before and after the reaction in the presence of SO_2. (**A**) MnZr; (**B**) MnCeZr; and (**C**) MnYZr. M: Surface metal or sulfur.

Table 2. Proportions of different O species obtained by the peak fitting of the O 1s curves.

Catalyst	O 1s 1	O 1s 2	O 1s 3	O 1s 4
MnZr	0.62	0.21	0.17	-
MnZr-SO_2	0.43	0.26	0.18	0.13
MnCeZr	0.15	0.32	0.24	0.29
MnCeZr-SO_2	0.29	0.20	0.28	0.23
MnYZr	0.33	0.36	0.30	-
MnYZr-SO_2	0.27	0.19	0.26	0.28

According to the results of XRD, H_2-TPR, and XPS, it was concluded that SO_2 combined with Ce or Y easily compared with Mn on the catalysts. Ce or Y inhibited the formation of manganese sulfate and protected the manganese active sites to some extent.

2.8. FTIR Analysis

To understand the role of Ce or Y better, FTIR experiments were performed. As shown in Figure 8, the spectrum of all fresh catalysts exhibited three characteristic peaks at 3440 cm^{-1}, corresponding to the vibration of –OH units [39–41]; at 1645 cm^{-1}, which was ascribed to the stretching vibration of C=C on the surface of MWCNTs [42]; and a broad peak in the 1000–400 cm^{-1} range, which was attributed to the stretching vibration of metallic oxide groups (Me–O–Me) [43,44]. Compared to the fresh catalysts, a peak around 1102 cm^{-1}, assigned to the SO_4^{2-} species, appeared after reacting with SO_2 [6,45]. From the partial magnification of corresponding FTIR spectra, the peak became weaker after loading Ce or Y, indicating that the addition of Ce or Y may prevent the manganese active sites from being sulfated to some extent [46].

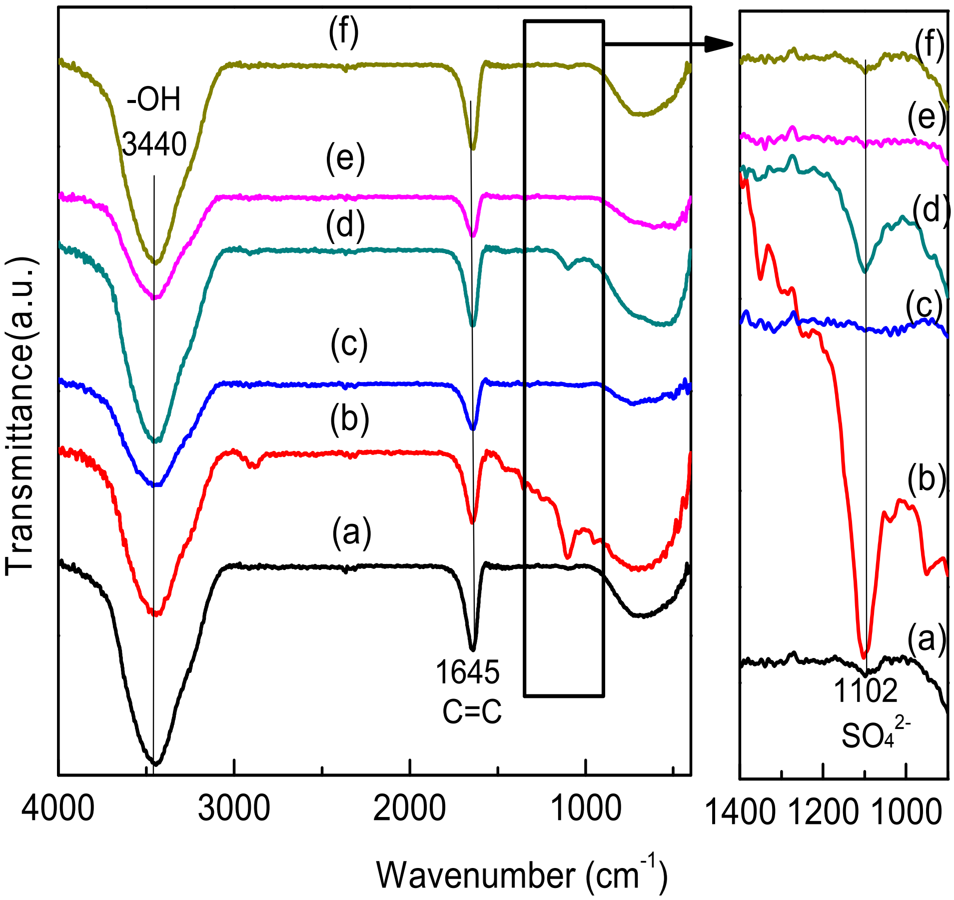

Figure 8. FTIR spectra of catalysts before and after the reaction in the presence of SO_2. (**a**) Fresh-MnZr; (**b**) used-MnZr; (**c**) fresh-MnCeZr; (**d**) used-MnCeZr; (**e**) fresh-MnYZr; and (**f**) used-MnYZr.

3. Materials and Methods

3.1. Pretreatment of MWCNTs

The MWCNTs were purchased from Shenzhen Nanotech Port Co. Ltd. (Shenzhen, China) According to Wang et al. [9], the MWCNTs were pretreated in HNO_3 solution by ultrasound for 30 min and heated at 100 °C for 4 h in a water-bath. Subsequently, MWCNTs were treated with filtration and washed by deionized water until the pH was neutral. The last sample was dried at 100 °C overnight for further use.

3.2. Preparation of MnO_x/ZrO_2/MWCNTs

The catalysts were prepared by step impregnation methods. Zirconium was supported on multi-wall carbon nanotubes (MWCNTs) to obtain zirconium-modified MWCNTs. The precursor was zirconium nitrate solution and zirconium loading was 30 wt. %. The sample were calcinated at 400 °C in an N_2 atmosphere for 2 h and denoted as ZrO_2/MWCNTs. Subsequently, to obtain MnO_x/ZrO_2/MWCNTs, 10 wt. % Mn was loaded on ZrO_2/MWCNTs by using the same method, for which the precursor was manganese nitrate. The detailed process has been previously described in Reference [47].

3.3. Preparation of Mn-CeO_x(YO_x)/ZrO_2/MWCNTS

MnO_x/ZrO_2/MWCNTs were introduced into a beaker containing 20 mL ethanol, and then stirred magnetically for 2 h. Cerium nitrate solution, used as the Ce precursor and controlled at 6 wt. % Ce loading with MWCNTS, was gradually added to the abovementioned mixture at room temperature and stirred for 3 h. The mixture was held under ultrasound for 30 min, then dried in the oven at 60 °C for 12 h. The powder was transferred to a tube furnace and calcined at 400 °C under N_2 for 2 h to obtain a Mn-CeO_x/ZrO_2/MWCNTS composite (denoted as MnCeZr). For comparison, Mn-YO_x/ZrO_2/MWCNTS (denoted as MnYZr) was prepared using yttrium nitrate as the Y precursor and controlling to 2 wt. % Y loading with MWCNTS by a similar method.

3.4. Catalytic Evaluations

The activity evaluation was carried out in a fixed-bed quartz continuous flow reactor under atmospheric pressure. 150 mg of the MnCeZr and MnYZr catalysts were used in the tests, respectively. The feed gas was composed of 0.06% NO, 0.06% NH3, 0.01% SO_2 (when added), 10% H_2O (when added) and 3.0% O_2 balanced by Ar. The total flow rate was 600 mL/min, corresponding to a gas hourly space velocity (GHSV) of 40,000 h^{-1}. The inlet and outlet concentrations of NO/NO_2 were analyzed by an online chemiluminescence NO-NO_2-NO_x analyzer (Thermal Scientific, model 42i-HL). The activity data were recorded when the reactions reached the steady state condition at each temperature. The reaction temperature was controlled from 80 to 300 °C with an isotherm step of 20 °C. The heating rate was about 5 °C/min. NO_x conversions were obtained by the following equation:

$$\delta(NO_x) = \frac{\varnothing(NO_x)_{in} - \varnothing\,(NO_x)_{out}}{\varnothing(NO_x)_{in}} \times 100\% \quad (2)$$

where $\delta(NO_x)$ represents the NO_x conversion; and $\phi\,(NO_x)_{in}$ and $\phi\,(NO_x)_{out}$ correspond to the inlet and outlet volume fraction of NO_x, respectively.

3.5. Catalyst Characterization

X-ray powder diffraction (XRD) patterns were recorded on a D8 Advace diffractometer (Bruker, Karlsruhe, Germany) with Cu Kα radiation (40 kV, 40 mA). Data were collected between 2θ = 10°–90° with 0.02° steps, and the XRD phases were identified by comparison with the reference data files from the Joint Committee on Power Diffraction Standards (JCPDS).

Hydrogen temperature-programmed reduction (H_2-TPR) of the catalyst was carried out on an Auto Chem II (Micromeritics, Gwinnett County, GA, USA). The samples were first flushed with Ar (30 mL/min) at 350 °C for 1 h. After that, the experiments were carried out at a heating rate of 10 °C/min from 60–700 °C in 10% H_2/Ar (30 mL/min). The H_2 consumption was recorded by a Thermal Conductivity Detector (TCD).

The chemical state and surface composition of the catalysts were analyzed by X-ray photoelectron spectroscopy (XPS, Axis Ultra DLD, Kratos, UK). All spectra were acquired at a basic pressure 3.33×10^{-6} Torr with Al Kα radiation (hv = 1253.6 eV) at 15 kV. The binding energy calibration was performed using the C 1s peak in the background as the reference energy (284.6 eV).

A Fourier transform infrared (FTIR) spectroscope (Nicolet 6700, Thermo Fisher Scientific, Waltham, MA, USA) was used to analyze the functional groups and determine the composition of the samples. Samples were achieved by pressing the mixture of catalysts and KBr. The weight ratio of catalysts : KBr was about 200. The FTIR measurements were performed at 4 cm^{-1} resolution with an accumulation of 64 scans.

4. Conclusions

The addition of Ce or Y loading on the MnO_x/ZrO_2/MWCNTs catalysts were prepared using the step impregnation method. Under simulated SCR reaction conditions, Ce improved the activity of the catalysts while the effect of Y was the opposite, however, they both enlarged the active temperature windows. The inhibition effect of H_2O on SCR activity was reversible, while the poisoning of SO_2 was more serious and irreversible when Ce or Y existed in the catalysts. This study found that the catalytic activity of MnCeZr was better than MnYZr in the abovementioned reaction conditions. Furthermore, Ce could improve the H_2O resistance of the catalysts to some extent, while the effect of Y was not obvious. For the MnCeZr catalysts, the coexistence of SO_2 and H_2O deactivated the catalysts more seriously than that in the presence of SO_2 or H_2O alone, implying that the co-existence of H_2O and SO_2 had a synergistic inhibition effect on SCR activity. Based on the results of XRD, H_2-TPR, XPS, and FTIR, Ce or Y existed in the catalysts in high dispersion or amorphous form. Ce could increase the mobility of the oxygen as well as the valence and oxidization of manganese while the effect of Y was the opposite, which may have been the main reason for the better catalytic activity of MnCeZr compared with MnYZr. Ce or Y combined with SO_2 easily to form sulfate species on the catalysts compared with Mn, then inhibited the formation of sulfate species and protected the manganese active sites to some extent, which was in accordance with the theory of ionic polarization.

Supplementary Materials: The following are available online at www.mdpi.com/2073-4344/7/6/181/s1, Figure S1: Ce 3d of catalysts before and after reaction in the presence of SO_2, Figure S2: Y 3d of catalysts before and after reaction in the presence of SO_2.

Acknowledgments: The project is financially supported by the National Natural Science Foundation of China (NSFC-51478191 and NSFC-20977034) and the Provincial Science and Technology Project (2014A020216003).

Author Contributions: Bichun Huang conceived and designed the experiments; Lifu Dong performed the experiments; Lifu Dong and Yinming Fan analyzed the data; Lifu Dong and Yinming Fan wrote the paper. Chao Yang and Wei Ling contributed reagents/materials/analysis tools.

Conflicts of Interest: The authors declare no conflict of interest.

References

1. Bosch, H.; Jamssen, F. Formation and control of nitrogen oxide. *Catal. Today* **1988**, *2*, 369–379.
2. Nova, I.; Ciardelli, C.; Tronconi, E.; Chatterjee, D.; Bandl-Konrad, B. NH_3-NO/NO_2 chemistry over V-based catalysts and its role in the mechanism of the Fast SCR reaction. *Catal. Today* **2006**, *114*, 3–12. [CrossRef]
3. Giakoumelou, I.; Fountzoula, C.; Kordulis, C.; Boghosian, S. Molecular structure and catalytic activity of V_2O_5/TiO_2 catalysts for the SCR of NO by NH_3: In situ Raman spectra in the presence of O_2, NH_3, NO, H_2, H_2O, and SO_2. *J. Catal.* **2006**, *239*, 1–12. [CrossRef]
4. Fan, X.Y.; Qiu, F.M.; Yang, H.S.; Tian, W.; Hou, T.F.; Zhang, X.B. Selective catalytic reduction of NO_x with ammonia over Mn-Ce-O_x/TiO_2-carbon nanotube composites. *Catal. Commun.* **2011**, *12*, 1298–1301. [CrossRef]
5. Kang, M.; Park, E.D.; Kim, J.M.; Yie, J.E. Manganese oxide catalysts for NO_x reduction with NH_3 at low temperatures. *Appl. Catal. A* **2007**, *327*, 261–269. [CrossRef]
6. Huang, J.H.; Tong, Z.Q.; Huang, Y.; Zhang, J.F. Selective catalytic reduction of NO with NH_3 at low temperatures over iron and manganese oxides supported on mesoporous silica. *Appl. Catal. B* **2008**, *78*, 309–314. [CrossRef]
7. Chen, Z.H.; Li, X.H.; Gao, X.; Jiang, Y.B.; Lu, Y.X.; Wang, F.R.; Wang, L.F. Selective catalytic reduction of NO_x with NH_3 on a Cr-Mn mixed oxide at low temperature. *Chin. J. Catal.* **2009**, *30*, 4–6. [CrossRef]
8. Xue, J.J.; Wang, X.Q.; Qi, G.S.; Wang, J.; Shen, M.Q.; Li, W. Characterization of copper species over Cu/SAPO-34 in selective catalytic reduction of NO_x with ammonia: Relationships between active Cu sites and de-NO_x performance at low temperature. *J. Catal.* **2013**, *297*, 56–64. [CrossRef]
9. Wang, L.S.; Huang, B.C.; Su, Y.X.; Zhou, G.Y.; Wang, K.L.; Luo, H.C.; Ye, D.Q. Manganese oxides supported on multi-walled carbon nanotubes for selective catalytic reduction of NO with NH_3: Catalytic activity and characterization. *Chem. Eng. J.* **2012**, *192*, 232–241. [CrossRef]
10. Pasel, J.; Kaβner, P.; Montanari, B.; Gazzano, M.; Vaccari, A.; Makowski, W.; Lojewski, T.; Dziembaj, R.; Papp, H. Transition metal oxides supported on active carbons as low temperature catalysts for the selective catalytic reduction (SCR) of NO with NH_3. *Appl. Catal. B* **1998**, *18*, 199–213. [CrossRef]
11. Tang, X.L.; Hao, J.M.; Yi, H.H.; Ning, P. Low-temperature SCR of NO with NH_3 on Mn-based Catalysts Modified with Cerium. *J. Rare Earths* **2007**, *25*, 240–243.
12. Jiang, B.Q.; Liu, Y.; Wu, Z.B. Low-temperature selective catalytic reduction of NO on MnO_x/TiO_2 prepared by different methods. *J. Hazard. Mater.* **2009**, *162*, 1249–1254. [CrossRef] [PubMed]

13. Smirniotis, P.G.; Pena, D.A.; Uphade, B.S. Low-temperature selective catalytic reduction (SCR) of NO with NH_3 by using Mn, Cr, and Cu oxides supported on hombikat TiO_2. *Ange. Chem. Int. Ed.* **2001**, *40*, 2479–2482. [CrossRef]
14. Pappas, D.K.; Boningari, T.; Boolchand, P.; Smirniotis, P.G. Novel manganese oxide confined interweaved titania nanotubes for the low-temperature Selective Catalytic Reduction (SCR) of NO_x by NH_3. *J. Catal.* **2016**, *334*, 1–13. [CrossRef]
15. Boningari, T.; Ettireddy, P.R.; Somogyvari, A.; Liu, Y.; Vorontsov, A.; McDonald, C.A.; Smirniotis, P.G. Influence of elevated surface texture hydrated titania on Ce-doped Mn/TiO_2 catalysts for the low-temperature SCR of NO_x under oxygen-rich conditions. *J. Catal.* **2015**, *325*, 145–155. [CrossRef]
16. Ettireddy, P.R.; Ettireddy, N.; Boningari, T.; Pardemann, R.; Smirniotis, P.G. Investigation of the selective catalytic reduction of nitric oxide with ammonia over Mn/TiO_2 catalysts through transient isotopic labeling and in situ FTIR studies. *J. Catal.* **2012**, *292*, 53–63. [CrossRef]
17. Thirupathi, B.; Smirniotis, P.G. Nickel-doped Mn/TiO_2 as an efficient catalyst for the low-temperature SCR of NO with NH_3: Catalytic evaluation and characterizations. *J. Catal.* **2012**, *288*, 74–83. [CrossRef]
18. Huang, B.; Huang, R.; Jin, D.; Ye, D. Low temperature SCR of NO with NH_3 over carbon nanotubes supported vanadium oxides. *Catal. Today* **2007**, *126*, 279–283. [CrossRef]
19. Qu, Z.; Miao, L.; Wang, H.; Fu, Q. Highly dispersed Fe_2O_3 on carbon nanotubes for low-temperature selective catalytic reduction of NO with NH_3. *Chem. Commun.* **2015**, *51*, 956–958. [CrossRef] [PubMed]
20. Wu, Z.B.; Jin, R.B.; Wang, H.Q.; Liu, Y. Effect of ceria doping on SO_2 resistance of Mn/TiO_2 for selective catalytic reduction of NO with NH_3 at low temperature. *Catal. Commun.* **2009**, *10*, 935–939. [CrossRef]
21. Jin, R.B.; Liu, Y.; Wu, Z.; Wang, H.B.; Gu, T.T. Relationship between SO_2 poisoning effects and reaction temperature for selective catalytic reduction of NO over Mn-Ce/TiO_2 catalyst. *Catal. Today* **2010**, *153*, 84–89. [CrossRef]
22. Li, Q.; Hou, X.X.; Yang, H.S.; Ma, Z.X.; Zheng, J.W.; Liu, F.; Zhang, X.B.; Yuan, Z.Y. Promotional effect of CeO_x for NO reduction over V_2O_5/TiO_2-carbon nanotube composites. *J. Mol. Catal. A* **2012**, *356*, 121–127. [CrossRef]
23. Ma, Z.X.; Yang, H.S.; Li, B.; Liu, F.; Zhang, X.B. Temperature-Dependent Effects of SO_2 on Selective Catalytic Reduction of NO over Fe-Cu-O_x /CNTs-TiO_2 Catalysts. *Ind. Eng. Chem. Res.* **2013**, *52*, 3708–3713.
24. Pan, S.W.; Luo, H.C.; Li, L.; Wei, Z.; Huang, B.C. H_2O and SO_2 deactivation mechanism of MnO_x/MWCNTs for low-temperature SCR of NO_x with NH_3. *J. Mol. Catal. A* **2013**, *377*, 154–161. [CrossRef]
25. Zhang, D.S.; Zhang, L.; Shi, L.Y.; Fang, C.; Li, H.R.; Gao, R.H.; Huang, L.; Zhang, J.P. In situ supported MnO_x-CeO_x on carbon nanotubes for the low-temperature selective catalytic reduction of NO with NH_3. *Nanoscale* **2013**, *5*, 1127–1136. [CrossRef] [PubMed]
26. Zhang, L.; Wang, D.; Liu, Y.; Kamasamudram, K.; Li, J.H.; Epling, W. SO_2 poisoning impact on the NH_3-SCR reaction over a commercial Cu-SAPO-34 SCR catalyst. *Appl. Catal. B* **2014**, *156–157*, 371–377. [CrossRef]
27. Busca, G.; Lietti, L.; Ramis, G.; Berti, F. Chemical and mechanistic aspects of the selective catalytic reduction of NO_x by ammonia over oxide catalysts: A review. *Appl. Catal. B* **1998**, *18*, 1–36. [CrossRef]
28. Thirupathi, B.; Smirniotis, P.G. Co-doping a metal (Cr, Fe, Co, Ni, Cu, Zn, Ce, and Zr) on Mn/TiO_2 catalyst and its effect on the selective reduction of NO with NH_3 at low-temperatures. *Appl. Catal. B* **2011**, *110*, 195–206. [CrossRef]
29. Dai, C.W. The thermal decomposition temperature of Sulphate of atomic steady potential scale. *Chin. J. Chem. Rev.* **1986**, *11*, 37–40.
30. Ettireddy, P.R.; Ettireddy, N.; Mamedov, S.; Boolchand, P.; Smirniotis, G.P. Surface characterization studies of TiO_2 supported manganese oxide catalysts for low temperature SCR of NO with NH_3. *Appl. Catal. B* **2007**, *76*, 123–134. [CrossRef]
31. Li, L.; Wang, L.S.; Pan, S.W.; Wei, Z.L.; Huang, B.C. Effects of cerium on the selective catalytic reduction activity and structural properties of manganese oxides supported on multi-walled carbon nanotubes catalysts. *Chin. J. Catal.* **2013**, *34*, 1087–1097. [CrossRef]
32. Koc, S.N.; Gurdag, G.; Geissler, S.; Muhler, M. Effect of nickel, lanthanum, and yttrium addition to magnesium molybdate catalyst on the catalytic activity for oxidative dehydrogenation of propane. *Ind. Eng. Chem. Res.* **2004**, *43*, 2376–2381. [CrossRef]

33. Zhang, D.S.; Zhang, L.; Fang, C.; Gao, R.H.; Qian, Y.L.; Shi, L.Y.; Zhang, J.P. MnO_x-CeO_x/CNTs pyridine-thermally prepared via a novel in situ deposition strategy for selective catalytic reduction of NO with NH_3. *RSC Adv.* **2013**, *3*, 8811–8819. [CrossRef]
34. Luo, H.C.; Huang, B.C.; Fu, M.L.; Wu, J.L.; Ye, D.Q. SO_2 Deactivation Mechanism of MnO_x /MWCNTs Catalyst for Low-Temperature Selective Catalytic Reduction of NO_x by Ammonia. *Acta Phys. Chim. Sin.* **2012**, *28*, 2175–2182.
35. Chang, H.Z.; Chen, X.Y.; Li, J.H.; Ma, L.; Wang, C.Z.; Liu, C.X.; Schwank, J.W.; Hao, J.M. Improvement of Activity and SO_2 Tolerance of Sn-Modified MnO_x-CeO_2 Catalysts for NH3-SCR at Low Temperatures. *Environ. Sci. Technol.* **2013**, *47*, 5294–5301. [CrossRef] [PubMed]
36. Guan, B.; Lin, H.; Zhu, L.; Huang, Z. Selective Catalytic Reduction of NO_x with NH_3 over Mn, Ce Substitution $Ti_{0.9}V_{0.1}O_{2-\delta}$ Nanocomposites Catalysts Prepared by Self-Propagating High-Temperature Synthesis Method. *J. Phys. Chem. C* **2011**, *115*, 12850–12863. [CrossRef]
37. Jin, R.; Liu, Y.; Wu, Z.; Wang, H.; Gu, T. Low-temperature selective catalytic reduction of NO with NH_3 over Mn Ce oxides supported on TiO_2 and Al_2O_3: A comparative study. *Chemosphere* **2010**, *78*, 1160–1166. [CrossRef] [PubMed]
38. Dupin, J.C.; Gonbeau, D.; Vinatier, P.; Levasseur, A. Systematic XPS studies of metal oxides, hydroxides and peroxides. *Phys. Chem. Chem. Phys.* **2000**, *2*, 1319–1324. [CrossRef]
39. Majumder, M.; Chopra, N.; Hinds, B.J. Effect of tip functionalization on transport through vertically oriented carbon nanotube membranes. *J. Am. Chem. Soc.* **2005**, *127*, 9062–9070. [CrossRef] [PubMed]
40. Liu, Y.Q.; Gao, L. A study of the electrical properties of carbon nanotube-$NiFe_2O_4$ composites: Effect of the surface treatment of the carbon nanotubes. *Carbon* **2005**, *43*, 47–52. [CrossRef]
41. Yu, C.L.; Wang, L.S.; Huang, B.C. In situ DRIFTS study of the low temperature selective catalytic reduction of NO with NH_3 over MnO_x supported on multi-walled carbon nanotubes catalysts. *Aerosol Air Qual. Res.* **2015**, *15*, 1017–1027. [CrossRef]
42. Yang, D.Q.; Rochette, J.F.; Sacher, E. Spectroscopic evidence for π-π interaction between poly(diallyl dimethylammonium) chloride and multiwalled carbon nanotubes. *J. Phys. Chem. B* **2005**, *109*, 4481–4484. [CrossRef] [PubMed]
43. Liu, Y.; Jiang, W.; Wang, Y.; Zhang, X.J.; Song, D.; Li, F.S. Synthesis of Fe_3O_4/CNTs magnetic nanocomposites at the liquid-liquid interface using oleate as surfactant and reactant. *J. Magn. Magn. Mater.* **2009**, *321*, 408–412. [CrossRef]
44. Shi, D.; Cheng, J.P.; Liu, F.; Zhang, X.B. Controlling the size and size distribution of magnetite nanoparticles on carbon nanotubes. *J. Alloys Comp.* **2010**, *502*, 365–370. [CrossRef]
45. Shen, B.X.; Zhang, X.P.; Ma, H.Q.; Yao, Y.; Liu, T. A comparative study of Mn/CeO_2, Mn/ZrO_2 and Mn/Ce-ZrO_2 for low temperature selective catalytic reduction of NO with NH_3 in the presence of SO_2 and H_2O. *J. Environ. Sci.* **2013**, *25*, 791–800. [CrossRef]
46. Jin, R.B.; Liu, Y.; Wang, Y.; Cen, W.L.; Wu, Z.B.; Wang, H.Q.; Weng, X.L. The role of cerium in the improved SO_2 tolerance for NO reduction with NH_3 over Mn-Ce/TiO_2 catalyst at low temperature. *Appl. Catal. B* **2014**, *148–149*, 582–588. [CrossRef]
47. Yang, C.; Liu, X.Q.; Huang, B.C.; Wu, Y.M. Structural properties and low-temperature SCR activity of zirconium-modified MnO_x/MWCNTs catalysts. *Acta Phys. Chim. Sin.* **2014**, *30*, 1895–1902.